

## Hardware-sensitive optimization for intensity modulated radiotherapy

Paul S Cho<sup>†</sup> and Robert J Marks II<sup>‡</sup>

<sup>†</sup> Department of Radiation Oncology, Box 356043, University of Washington, Seattle, WA 98195-6043, USA

<sup>‡</sup> Department of Electrical Engineering, University of Washington, Seattle, WA 98195-2500, USA

E-mail: cho@radonc.washington.edu

Received 22 July 1999, in final form 12 October 1999

**Abstract.** The multileaf collimator (MLC) hardware constraints are usually neglected in the process of intensity-modulated beam optimization. Consequently, it is not always possible to deliver planned beam modulation using dynamic MLC. Beam optimization is significantly diminished if the results must be approximated due to limitations imposed by the delivery device. To overcome this problem, an inverse beam optimization method which incorporates the hardware constraints has been developed. The hardware constraints, including the leaf velocity, the dose rate and the minimum required gap between opposing and adjacent leaves, were considered. An iterative search for feasible modulation was conducted alternately in the dosimetric space and the MLC position–time space. The optimization algorithm was designed for a unidirectional leaf trajectory and a constant dose rate. A scheme to reduce tongue-and-groove underdosage during optimization was also implemented. Comparisons were made between the solutions produced by this method and conventional optimization disregarding the hardware restrictions. The beam profiles generated by the conventional method were modified to satisfy the hardware specifications. The results indicate that inclusion of MLC constraints during optimization can improve the degree of conformity that is deliverable.

### 1. Introduction

A number of approaches have been proposed to solve the problem of inverse optimization in radiotherapy. Dictated by the available technology, early works have assumed predetermined intensity profiles (uniform or wedged fields) and focused on the selection of beam weights. Determination of beam weights was performed using various optimization techniques including linear programming (Bahr *et al* 1968), quadratic programming (Redpath *et al* 1976), least-squares (McDonald and Rubin 1977) and constrained least-squares methods (Starkschall 1984). A fully discretized formulation of the inverse radiotherapy problem was introduced by Censor *et al* (1988) in which each beam was quantized into rays. Although the individual ray weights were summed to rank the prominence of each beam, their work has laid a foundation for computer-controlled MLC technology capable of generating arbitrary intensity modulation. More recently, the advent of the MLC-based conformal radiotherapy technology has spurred the development of inverse techniques for multi-beam-element multiple-beam configurations. A wide variety of methods have been described, including simulated annealing (Webb 1989), steepest descent (Lind 1990), quasi-Newton (Bortfeld *et al* 1990), iterative filtered backprojection (Holmes *et al* 1991), projections onto convex sets (Lee *et al* 1997),

conjugate gradient (Hristov and Fallone 1997) and variation (Liu *et al* 1999). While these methods were designed to optimize dosimetric objectives and constraints, few techniques have been formulated to optimize radiobiological indices (Källman *et al* 1992, Raphael 1992, Gustafsson *et al* 1994). Comparisons of some of these algorithms have also been reported (Holmes and Mackie 1994, Xing and Chen 1996, Cho *et al* 1997).

The assumption common to these techniques is that the optimized beam profiles can be accurately delivered by the beam modulation hardware. However, due to mechanical restrictions certain modulation patterns are difficult or even impossible to realize with the currently available MLC hardware. For example, the minimum gap between the opposing leaves required by some machines determines the location of the earliest appearance of the negative fluence gradient<sup>†</sup> in the modulation. The reason is that the leading (right) leaf, which is needed to generate negative gradient, cannot be placed closer to the trailing leaf than the gap separation. Therefore, if the starting location of the trailing leaf defines the field edge, the position of the first negative gradient must be at least the required gap away from the field edge. The exception to this rule occurs when the trailing back-up diaphragm is available to define the field edge, permitting the trailing leaf to be positioned behind the diaphragm and the leading leaf at the field border. However, the use of a back-up diaphragm, which is usually thinner than the MLC, could result in delivery errors.

The problem of leaf gap is further compounded if the opposing leaves in the adjacent tracks are also required to maintain a minimum separation in order to prevent interdigitation. The minimum gap restriction between adjacent tracks disallows large differences in intertrack modulation. Another problem is the generation of zero-intensity valleys when the leaf pairs are not permitted to close completely. In addition, the upper limit on leaf velocity determines the minimum gradient achievable by a single leaf for a given dose rate and dictates the modulation within the segments where only one of the paired leaves is available due to the minimum leaf gap requirement.

Impetus for incorporating the hardware parameters in IMRT optimization also comes from practical considerations. For example, in theory, even extremely shallow fluence valleys can be delivered using low dose rates that approach zero. However, in practice, use of low dose rates could lead to unstable machine output and frequent beam interrupts resulting in inaccurate delivery. Therefore, it is advantageous to be able to specify the dose rate during the optimization process so that at the time of fluence-to-leaf sequencing translation, no dose rate below a certain practical limit needs to be used.

Beam optimization is significantly diminished if the results have to be approximated due to limitations imposed by the beam modulation hardware. To overcome this problem, an inverse beam optimization method which incorporates the MLC hardware constraints has been developed. The hardware parameters considered in the present investigation include maximum leaf velocity, dose rate, minimum gap and leaf synchronization for reduction of tongue-and-groove underdosage.

## 2. Methods

In the following it is assumed that the leaves traverse monodirectionally from left to right and the dose rate is constant. Furthermore, in order to maintain generality of the method it is assumed that the back-up diaphragms are not available for beam modulation purposes. They are positioned so as to form a bounding box encompassing the field edges.

<sup>†</sup> The sign convention is such that the gradient is negative when the fluence is decreasing in the direction of leaf travel and positive otherwise.

Analyses of modulation profiles for leaf speed, dose rate, gap requirement and tongue-and-groove effects are most conveniently performed in the MLC position–time space. The position–time space describes the leaf position as a function of cumulative MU. When the dose rate  $\Phi$  is kept constant the cumulative MU equals time. Violation of minimum leaf gap within the same track and between adjacent tracks is detected by checking the distance between curves along the leaf position axis. The gradient of the position–time curve provides the measure of leaf velocity. Furthermore, the extent of tongue-and-groove underdosage can be evaluated in terms of the degree of curve synchronization.

The search for a feasible solution is accomplished by the method of projections onto convex sets (POCS) (Lee *et al* 1997, Cho *et al* 1997, 1998). The basic strategy is to switch between the dose space and the position–time space during the optimization process. Dosimetric constraints are handled in the dose space as described previously (Cho *et al* 1998) while the MLC hardware parameters are considered in the MLC position–time domain. Here, we will focus on the formulation of the MLC constraints in position–time space.

The adjoining of all the left ( $l$ ) and the right ( $r$ ) leaf positions over time serves as points in a Hilbert space

$$\mathcal{H} = \{l_i(t), r_i(t) \mid 1 \leq i \leq N, 0 \leq t \leq T\} \quad (1)$$

where the inner product and norm are defined in the conventional manner (Naylor and Sell 1982),  $i$  is the MLC leaf number ranging from 1 to  $N$ , and  $T$  is the total delivery time. MLC constraints can be formulated in this space.

### 2.1. Velocity constraint

A set of leaf velocities that are less than a certain maximum form a convex set

$$C_v = \{l_i(t), r_i(t) \mid \dot{l}_i \leq V_{\max}/\Phi, \dot{r}_i \leq V_{\max}/\Phi\}. \quad (2)$$

For a given leaf trajectory velocities in excess of  $V_{\max}/\Phi$  are reduced to the maximum possible speed. In terms of leaf position the projection is

$$\mathcal{P}_v[l_i(t), r_i(t)] = \left\{ \int_0^t \dot{l}_i(\tau) d\tau, \int_0^t \dot{r}_i(\tau) d\tau \right\} \quad (3)$$

where

$$\dot{l}_i(\tau) = \begin{cases} V_{\max}/\Phi & dl_i/dt > V_{\max}/\Phi \\ 0 & dl_i/dt < 0 \\ \dot{l}_i & \text{otherwise} \end{cases} \quad (4)$$

$$\dot{r}_i(\tau) = \begin{cases} V_{\max}/\Phi & dr_i/dt > V_{\max}/\Phi \\ 0 & dr_i/dt < 0 \\ \dot{r}_i & \text{otherwise.} \end{cases} \quad (5)$$

Note that since a monodirectional trajectory is assumed, negative velocities are disallowed.

### 2.2. Gap constraint

The opposing leaves whose separations are greater than a certain minimum value,  $g$ , comprise a convex set. For the leaves within the same track the set is given by

$$C_{S_1} = \{l_i(t), r_i(t) \mid r_i(t) - l_i(t) \geq g\} \quad (6)$$

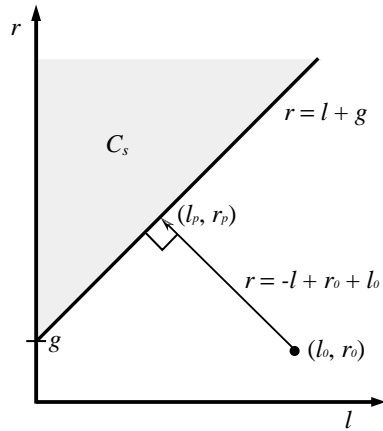


**Figure 1.** Projection onto the minimum gap constraint set,  $C_s$  (shaded). The point  $(l_o, r_o)$  violates the gap constraint. Its projected point  $(l_p, r_p)$  is the intersection of  $r = l + g$  and  $r = -l + r_o + l_o$ .

and between the adjacent tracks

$$C_{S_2} = \{l_i(t), r_{i-1}(t) \mid r_{i-1}(t) - l_i(t) \geq g\}. \quad (7)$$

For a given time  $t$ ,  $l(t)$  and  $r(t)$  are orthogonal<sup>†</sup>. The projection onto the gap constraint set is depicted in figure 1. If a set of left and right leaf positions already exists in the constraint set (shaded region), then the projection is onto itself. If, however, the leaf positions are outside of the constraint set, as illustrated by the point  $(l_o, r_o)$ , the projection point  $(l_p, r_p)$  is the point on the set which is closest to  $(l_o, r_o)$ , i.e. the intersection between the constraint set boundary  $r = l + g$  and the orthogonal vector along the line  $r = -l + r_o + l_o$ . Solving the equations, we get  $l_p = (r_o + l_o - g)/2$  and  $r_p = (r_o + l_o + g)/2$ . In general terms the projection is given by

$$\mathcal{P}_{S_1}[l_i(t), r_i(t)] = \begin{cases} l_i(t) + (r_i(t) - l_i(t) - g)/2 & \text{for } l_i \\ r_i(t) - (r_i(t) - l_i(t) - g)/2 & \text{for } r_i \end{cases} \quad (8)$$

and

$$\mathcal{P}_{S_2}[l_i(t), r_{i-1}(t)] = \begin{cases} l_i(t) + (r_{i-1}(t) - l_i(t) - g)/2 & \text{for } l_i \\ r_{i-1}(t) - (r_{i-1}(t) - l_i(t) - g)/2 & \text{for } r_{i-1}. \end{cases} \quad (9)$$

Any reversal in leaf direction that may arise from this projection will be corrected by the non-negative velocity condition imposed by the projection operation given in equation (3).

### 2.3. Tongue-and-groove constraint

The tongue-and-groove effects occur when adjacent leaves shuffle ahead of each other. As a result, narrow overlapping shadows are generated leading to underdosage errors. The errors can be minimized through synchronization of adjacent leaves (van Santvoort and Heijmen 1996). This can be accomplished by synchronizing the position-time curves of either the leading or the trailing leaves of the adjacent tracks. Here, the formulation is presented using the notation for the trailing (left) leaves.

For a given  $n$  such that  $1 < n \leq N$ , the set

$$\mathcal{S}_n = \{l_n(t), l_{n-1}(t) \mid 0 \leq t \leq T\} \quad (10)$$

<sup>†</sup> In other words,  $\{l(t), 0\} \in \mathcal{H}$  is orthogonal to every  $\{0, r(t)\} \in \mathcal{H}$ .

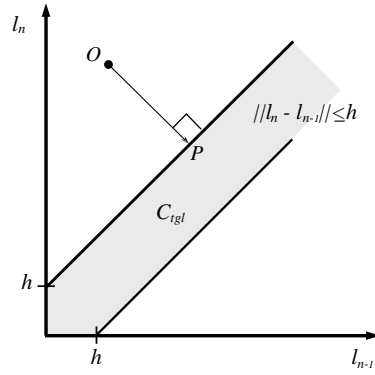


**Figure 2.** Projection onto the tongue-and-groove constraint set,  $C_{tgl}$  (shaded). Similarly to figure 1, the projected point  $P$  is at the minimum distance from the point  $O$  representing unsynchronized leaf positions.

is a subspace of  $\mathcal{H}$ . Define the convex set in  $\mathcal{S}_n$  (and thus in  $\mathcal{H}$ ) as

$$C_{tgl} = \{l_n(t), l_{n-1}(t) \in \mathcal{S}_n \mid \|l_n(t) - l_{n-1}(t)\| \leq h(t)\}. \quad (11)$$

This represents a set of adjacent leaf positions of separations less than or equal to  $h(t)$ . Full synchronization is achieved when  $h(t) = 0$ . In practice,  $h(t)$  is given by

$$h(t) = (l_n(t) - l_{n-1}(t))/q \quad (12)$$

where  $q \geq 1$  is a relaxation parameter which controls the degree of leaf synchronization.

As shown in figure 2, projection of the leaf coordinates lying outside the constraint set denoted by the point  $O$  can be derived geometrically by finding the intersection between the set  $C_{tgl}$  and the minimum distance vector  $\vec{OP}$  yielding

$$\mathcal{P}_{tgl}[l_n(t), l_{n-1}(t)] = \begin{cases} l_n(t) - (l_n(t) - l_{n-1}(t) - h(t))/2 & \text{for } l_n \\ l_{n-1}(t) + (l_n(t) - l_{n-1}(t) - h(t))/2 & \text{for } l_{n-1}. \end{cases} \quad (13)$$

#### 2.4. Beam-to-trajectory transformation

The convex projection operations for the MLC hardware constraints begin by mapping the MU (machine monitor unit)-position functions  $f(x)$  into MLC leaf trajectory space. Assuming the left-to-right, monodirectional leaf trajectory, the positive fluence gradient is generated by the left leaf and the negative gradient by the right. The process of fluence decomposition into left and right leaf trajectories following this paradigm is accomplished by

$$\mathcal{P}_{wl}[f_i(x)] = l_i^{-1}(x) = \left\{ \int^x f_i'(\tilde{x}) \mu(f_i'(\tilde{x})) d\tilde{x} \right\} \quad (14)$$

and

$$\mathcal{P}_{wr}[f_i(x)] = r_i^{-1}(x) = \left\{ \int^x -f_i'(\tilde{x}) \mu(-f_i'(\tilde{x})) d\tilde{x} \right\} \quad (15)$$

where  $\mu(\cdot)$  is a unit step function which is equal to 1 when its argument is positive and 0 otherwise. The outer negative sign in equation (15) puts the right leaf trajectory in the positive fluence space. In other words,  $r_i^{-1}(x)$  represents fluence blocked by the right leaf rather than the negative fluence generated. The fluence at position  $x$  is recovered by  $l_i^{-1}(x) - r_i^{-1}(x)$ .

The resultant time–position functions are monotonically increasing and can be inverted to form more convenient position–time functions,  $l_i(t)$  and  $r_i(t)$ . Subsequent projections of the position–time values onto the velocity constraint set will remove violations including infinite velocity arising from the zero-gradient segments<sup>†</sup>.

### 2.5. Iterative projections

The above operations are repeated during the iterative optimization to guide the solution to remain within the realizable limits set by the specific MLC hardware. The overall inverse beam design consists of both dosimetric and trajectory optimization as outlined below, beginning with an estimation of the initial beam-element weights (steps I-1 through I-3). Iterative projections are described in steps L-1 through L-10. For detailed description of convex projections used in steps L-1, 2 and 3, readers are referred to Cho *et al* (1998).

I-1 Set the dose points within the target volume to the prescribed dose.

I-2 Obtain initial beam-element weights using the pseudo-inversion method given by

$$\vec{b} = \frac{\mathbf{A}^T \vec{d}}{\|\mathbf{A}\|^2} \quad (16)$$

where  $\vec{b}$  represents a vector of beam-element weights,  $\vec{d}$  consists of doses at sampling points and the matrix  $\mathbf{A}$  specifies the dose contribution per unit weight from a beam element to each of the dose points.

I-3 Calculate the dose for all sampling points within the entire volume.

L-1 Compute the changes in dosage necessary to satisfy the target prescription.

L-2 Compute the changes in dosage necessary to satisfy organ protection goals.

L-3 Compute the equivalent changes in beam-element weights using equation (16) and update the current beam-element weights.

L-4 Transform beam-element weights to position–time functions using equations (14) and (15).

L-5 Impose the leaf velocity constraint using equation (3).

L-6 Impose the MLC gap constraint using equations (8) and (9).

L-7 Apply leaf synchronization using equation (13).

L-8 Transform position–time functions to beam-element weights.

L-9 Compute the dose at sampling points.

L-10 If the termination condition is met, exit, else loop back to L-1.

If some of the constraint sets do not intersect, iterative projections will eventually reach a limit cycle at which point no further improvement in convergence will occur. This condition represents no improvement in the mean-square distance between projections and is detectable by the algorithm.

The algorithm was tested using a simulated tumour–organ geometry. The height of the tumour–organ volume was 6 cm. The tumour shape changes at the mid-height as shown in figure 3. Eight equiangular 6 MV beams were used. The beam-element resolution at the isocentre was  $0.25 \times 1.0 \text{ cm}^2$ . Beam elements were computed with a modified convolution/superposition method using multiresolution kernel sampling (Sutlief *et al* 1998).

<sup>†</sup> Normally, in leaf sequencing the problem with zero gradient is circumvented by applying a shear operator (Boyer and Strait 1997) which effectively increases the entire trajectory by  $x/V_{\max}$  thus replacing the zero-gradient segments with the minimum allowable.

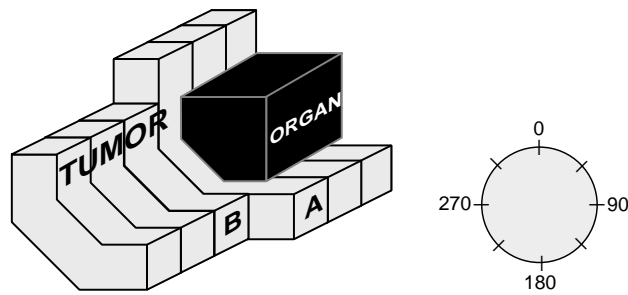


**Figure 3.** A cut-away view of the tumour–organ structure used in algorithm testing. Note the abrupt change in tumour geometry between transaxial slices A and B. The organ volume extends for the entire tumour height. Eight equiangular beams were placed from  $0^\circ$  to  $315^\circ$ .

For the purpose of beam optimization, contributions from each beam element to dose sampling points including 3D scatter were precomputed and stored in an array representing the **A** matrix in equation (16). Dose sampling points were distributed uniformly in  $0.2 \times 0.2 \times 1.0$  cm increments. Calibration of relative fluence to MU was performed through preliminary optimization during which the hardware-specific constraints requiring the knowledge of MU (steps L-4 through L-8) were turned off. The resultant photon fluence values were converted to MU using the tissue phantom ratios, relative output factor, and machine cGy/MU calibration data. The fluence-to-MU conversion factor thus derived was used in the subsequent optimization process with the MLC constraints enabled. The following MLC parameters were used: maximum leaf velocity of  $2 \text{ cm s}^{-1}$ , minimum gap of 1 cm between opposing leaves within the same track and adjacent tracks, and dose rate of  $400 \text{ MU min}^{-1}$ .

In order to compare the present technique with a conventional method, beam optimization for the test geometry was also performed without considering the MLC hardware limitations. For either case, with and without the hardware constraints enabled, the optimization goal was to achieve a total of 85 Gy to the entire target volume while minimizing the dose to the critical structure. Choice of the prescription dose is arbitrary and is not critical for the purpose of algorithm demonstration.

### 3. Results

Interdigitation and gap violation are likely to occur when there is a large change in irradiated anatomy. In the test case shown this occurs for the MLC tracks A and B between which there is a maximum change of 2 cm in the tumour dimension. The results of conventional beam optimization disregarding the hardware constraints showed the gap violations in all eight beam orientations. Here, selected examples are presented to illustrate the efficacy of the present algorithm.

Figure 4 corresponds to track B of the beam at  $225^\circ$  relative to figure 3. Figure 4(a) shows the beam profile (per fraction) generated by the conventional optimization. Transformation of the profile into MLC time–position curves reveals that the minimum gap requirement is violated as indicated by the arrow in figure 4(c). The problematic trajectory segment corresponds to the low-fluence valley in figure 4(a). On the other hand, the MLC-sensitive optimization has generated a modulation pattern with a slightly shallower fluence valley (figure 4(b)) which is deliverable. The associated MLC trajectory shows that the minimum gap distance of 1 cm is maintained throughout the delivery (figure 4(d)).

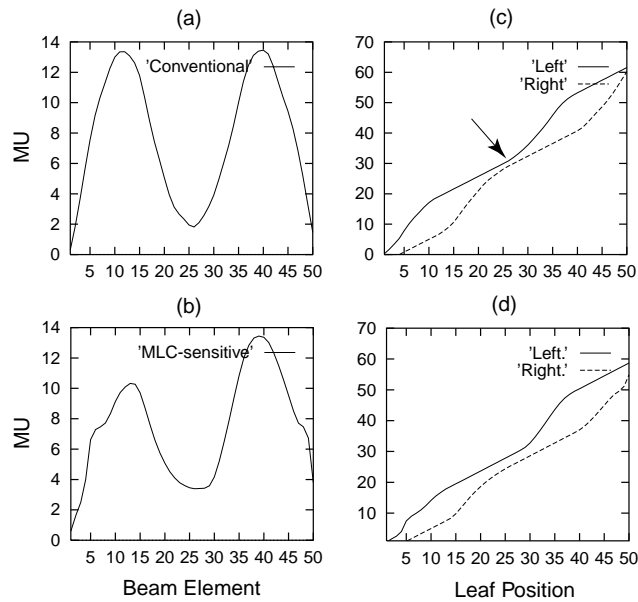


**Figure 4.** Example of optimization results; track B of the beam at  $225^\circ$  orientation relative to figure 3 (one beam element = one leaf position = 0.25 cm): (a) beam profile generated by the conventional optimization disregarding hardware constraints; (b) beam profile generated by the hardware-sensitive optimization method; (c) leaf trajectory of the modulation shown in (a). The arrow indicates violation of minimum gap requirement. (d) Leaf trajectory of the modulation shown in (b).

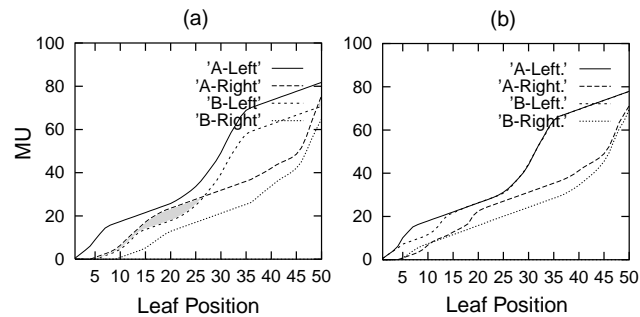


**Figure 5.** Example of optimization results; tracks A and B of the beam at  $90^\circ$ : (a) conventional optimization exhibiting interdigitation (shaded regions). (b) hardware-sensitive optimization.

Figure 5 shows the MLC trajectories for the adjacent tracks A and B of the beam at  $90^\circ$  orientation. The curves for the conventional optimization are given in figure 5(a) which illustrates the interdigitation between the leading leaf of track B and trailing leaf of track A (shaded regions). In contrast, the trajectories representing the hardware-sensitive optimization are free of leaf collision (figure 5(b)). Figure 5(b) also demonstrates that the leaves are almost fully synchronized for this beam. Overall, full synchronization was achieved in six out of the eight beams.

The MLC time–position sequences resulting from the conventional optimization were corrected for collision by ensuring the required gap at the start and thereafter by slowing

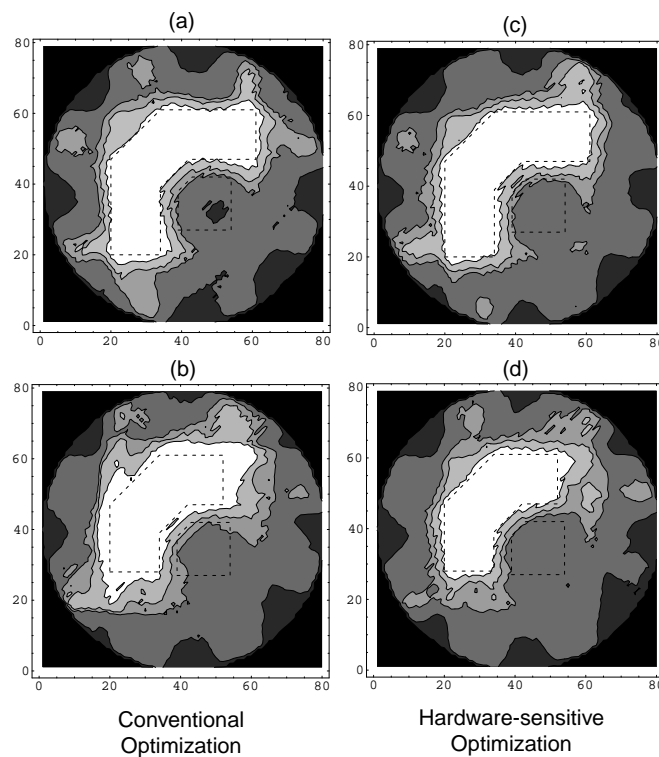


**Figure 6.** Isodose distribution generated from the beam modulation optimized with and without considering MLC hardware constraints. The 85 Gy, 70 Gy, 60 Gy, 30 Gy and 5 Gy isodose lines are shown. The broken lines indicate the target boundary. (a) isodose plots for slice A generated by the conventional optimization; (b) plots for slice B; (c) isodose plots for slice A generated by the hardware-sensitive optimization; (d) plots for slice B.

down the trailing leaves and/or speeding up the leading leaf within the limit of  $3.33 \text{ MU cm}^{-1}$  imposed by the dose rate of  $400 \text{ MU min}^{-1}$  and the maximum leaf speed of  $2.0 \text{ cm s}^{-1}$ . In order to assess the effects of the post-optimization gap correction, the isodose distributions resulting from the revised leaf trajectories were computed as shown in figures 6(a) and 6(b). In calculating the dose it was assumed that the back-up diaphragms defining the vertical field boundary remained stationary and the leading leaves were allowed to sweep over the diaphragm to prevent collision at the finish of the delivery. Radiation transmission through the blocking devices and penumbra effects were not considered. Likewise, the isodose distributions for the MLC-sensitive optimization results were calculated; these are shown in figures 6(c) and 6(d). Comparison of the isodose curves generated by the two methods reveal similar dose distributions for the plane corresponding to the tumour–organ geometry along MLC track A (figures 6(a) and 6(c)). However, in the adjacent plane corresponding to track B appreciable overdosage around the target is noted when post-optimization gap correction was applied to the conventional technique (figure 6(b)). On the other hand, much more conformal dose distribution is observed for the hardware-sensitive beam optimization (figure 6(d)).

The program was coded in C and executed on a computer configured with a 233 MHz Pentium-II processor under the Linux operating system. Convergence to the solution was achieved in 200 iterations and 91 s.

#### 4. Discussion

We have demonstrated that the process of inverse beam optimization could lead to a solution which cannot be delivered if the hardware limitations are neglected during optimization. The proposed algorithm overcomes the problem by incorporating the MLC constraints in the process of inverse optimization itself. A feasible solution was obtained from a search space limited in possible leaf trajectories as defined by machine-specific maximum leaf speed, minimum leaf separation and available range of dose rate. The dose distribution resulting from the hardware-sensitive beam calculation yielded more conformal isodose curves than those from the conventional method corrected for deliverability after optimization. This suggests that over- or underexposure introduced by the restricted leaf trajectory in one beam angle can be compensated by the modulation from other beam angles. As such, significant reduction in number of beams might result in reduced conformity when hardware constraints are applied.

The constraints were formulated either in MLC position-time space or dose space as convex sets. The interchange between the two domains was accomplished in two steps. First, transformation from dose to beam space was performed by equation (16) which is itself a convex projection as previously proven (Lee *et al* 1997). Second, transformation from beam to leaf trajectory space was carried out using equations (14) and (15). The operation performed to impose monotonicity is not, in the strict sense, a projection onto the convex set of strictly increasing positive functions. It does, however, impose the constraint of monotonicity onto the fluence function in a straightforward manner and was shown to be an effective component operation useful in the otherwise POCS framework.

The minimum gap requirement was imposed as a hard constraint since this condition cannot be violated by the delivery device. On the other hand, the tongue-and-groove error correction was applied as a soft constraint. A strict demand for full synchronization could reduce the dose conformity by competing with the dosimetric objectives and constraints. Compared with the correction driven by the minimum gap constraint which is usually applied only to parts of the trajectories, a full synchronization would likely require alteration of the entire trajectory and thus the entire beam profile. It should be noted that unlike the synchronization method used in fluence-to-trajectory translation in which the original modulation is unchanged by slowing down the opposing unsynchronized leaves, the present method of synchronization does not attempt to preserve the modulation. To do so would accomplish nothing in the iterative process. Rather, the present operation is designed to perturb the modulation toward production of synchronized trajectories. The residual tongue-and-groove errors can be reduced after the optimization at the expense of increased delivery time (van Santvoort and Heijmen 1996). The soft constraint was implemented by reducing the trajectory difference by a fraction rather than the full separation between the leaves. The size of the fraction was set by the relaxation parameter  $q$  in equation (12). For the example shown,  $q$  was set to 10.

Recently, a new class of fluence-to-leaf sequencing translator has been developed in order to overcome the problem of minimum gap requirements (Convey and Webb 1998, Kuterdem *et al* 1999). These algorithms exploit the capability of machines equipped with computer-controlled back-up diaphragms which can be manipulated independently of MLC. The gap problem can be avoided if one of the violating leaves could be replaced by a back-up diaphragm. It should be noted, however, that the use of back-up diaphragms could lead to delivery errors due to increased transmission. For example, using the 6 MV photon beam we measured the transmission factor of 10.4% for the back-up diaphragms which move in parallel to the MLC. In comparison, the radiation transmission for the MLC is 1.8%. These values agree well with the published data (Jordan and Williams 1994). Therefore, beam blocking by the back-up

diaphragms alone without overlapping MLC could be large. Since the present optimization method relies solely on MLC to modulate the beam, the transmission errors can be kept to a minimum. Furthermore, in case of complex modulations, even with the help of an additional blocking device it may not be possible to accurately generate intended fluence patterns unless beam pauses are inserted. Beam interrupts are not yet practical as the pulse stabilization process is still very slow in currently available accelerators. For example, up to 15 seconds of pause recovery time has been reported in IMRT beam delivery with a magnetron-based machine (Kuterdem *et al* 1999).

The effects of penumbra, head scatter, radiation transmission through leaves and back-up diaphragms were not considered in conjunction with the beam optimization process. Correction for these effects can be handled in the subsequent conversion step of fluence to leaf sequencing. The leaf trajectories can be modified to account for these effects through an iterative process such as described by Convery and Webb (1997, 1998) and implemented by Dirkx *et al* (1997, 1998). In such a process the input to the fluence-to-trajectory translator is adjusted according to the difference between the desired (output of the inverse beam optimization) and the computed fluence from the resultant trajectory including the above effects. The process is iterated few times until the discrepancy is minimized. As noted above, correction due to transmission should be small for the present method which does not require back-up diaphragms to modulate beam intensity.

## 5. Conclusion

An inverse beam optimization algorithm was formulated which incorporates the knowledge of beam modulation hardware specifications. The results indicate that inclusion of MLC hardware constraints during optimization can improve the degree of conformity that is deliverable.

## Acknowledgments

This work was supported in part by a grant from the Whitaker Foundation. The authors are grateful to Steve G Sutlief PhD for providing the convolution/superposition dose computation program.

## References

- Bahr G K, Kereiakes J G, Horwitz H, Finney R, Galvin J and Goode K 1968 The method of linear programming applied to radiation treatment planning *Radiology* **91** 686–93
- Bortfeld T, Burkelbach J, Boesecke R and Schlegel W 1990 Methods of image reconstruction from projections applied to conformation radiotherapy *Phys. Med. Biol.* **35** 1423–34
- Boyer A L and Strait J P 1997 Delivery of intensity-modulated treatments with dynamic multileaf collimators *Proc. 12th Int. Conf. on Computers in Radiotherapy (Utah, May 1997)* ed D D Leavitt and G Starkschall (Madison, WI: Medical Physics Publishing) pp 13–15
- Censor Y, Altschuler M D and Powlis W D 1988 On the use of Cimmino's simultaneous projections method for computing a solution of the inverse problem in radiation therapy treatment planning *Inverse Problems* **4** 607–23
- Cho P S, Lee S, Marks II R J, Oh S, Sutlief S G and Phillips M H 1998 Optimization of intensity modulated beam with volume constraints using two methods: cost function minimization and projections onto convex sets *Med. Phys.* **25** 435–43
- Cho P S, Lee S, Marks II R J, Redstone J A and Oh S 1997 Comparison of algorithms for intensity modulated beam optimization: projections onto convex sets and simulated annealing *Proc. 12th Int. Conf. on Computers in Radiotherapy (Utah, May 1997)* ed D D Leavitt and G Starkschall (Madison, WI: Medical Physics Publishing) pp 310–12

- Convery D J and Webb S 1997 Calculation of the distribution of head-scattered radiation in dynamically-collimated MLC fields *Proc. 12th Int. Conf. on Computers in Radiotherapy (Utah, May 1997)* ed D D Leavitt and G Starkschall (Madison, WI: Medical Physics Publishing) pp 350–3
- 1998 Generation of discrete beam-intensity modulation by dynamic multileaf collimation under minimum leaf separation constraints *Phys. Med. Biol.* **43** 2521–38
- Dirkx M L P, Heijmen B J M and van Santvoort J P C 1997 Optimization of leaf trajectories for dynamic multileaf collimation to realise desired intensity modulated beam profiles *Proc. 12th Int. Conf. on Computers in Radiotherapy (Utah, May 1997)* ed D D Leavitt and G Starkschall (Madison, WI: Medical Physics Publishing) pp 357–9
- 1998 Leaf trajectory calculation for dynamic multileaf collimation to realize optimized fluence profiles *Phys. Med. Biol.* **43** 1171–84
- Gustafsson A, Lind B K and Brahme A 1994 A generalized pencil beam algorithm for optimization of radiation therapy *Med. Phys.* **21** 343–56
- Holmes T and Mackie T R 1994 A comparison of three inverse treatment planning algorithms *Phys. Med. Biol.* **39** 91–106
- Holmes T, Mackie T R, Simpkin D and Reckwerdt P 1991 A unified approach to the optimization of brachytherapy and external beam dosimetry *Int. J. Radiat. Oncol. Biol. Phys.* **20** 859–73
- Hristov D H and Fallone B G 1997 An active set algorithm for treatment planning optimization *Med. Phys.* **24** 1455–64
- Jordan T J and Williams P C 1994 The design and performance characteristics of a multileaf collimator *Phys. Med. Biol.* **39** 231–51
- Källman P, Lind B K and Brahme A 1992 An algorithm for maximizing the probability of complication-free tumour control in radiation therapy *Phys. Med. Biol.* **37** 871–90
- Kuterderm H G, Cho P S and Marks II R J 1999 Dynamic multileaf-diaphragm sequencing with adjacency gap constraints *Med. Phys.* **26** 1136 (abstract)
- Lee S, Cho P S, Marks II R J and Oh S 1997 Conformal radiotherapy computation by the method of alternating projections onto convex sets *Phys. Med. Biol.* **42** 1065–86
- Lind B K 1990 Properties of an algorithm for solving the inverse problem in radiation therapy *Inverse Problems* **6** 415–26
- Liu Y, Yin F and Gao Q 1999 Variation method for inverse treatment planning *Med. Phys.* **26** 356–63
- McDonald S C and Rubin P 1977 Optimization of external beam radiation therapy *Int. J. Radiat. Oncol. Biol. Phys.* **2** 307–17
- Naylor A W and Sell G R 1982 *Linear Operator Theory in Engineering and Science* 2nd edn (New York: Springer) pp 272–344
- Raphael C 1992 Mathematical modelling of objectives in radiation therapy treatment planning *Phys. Med. Biol.* **37** 1293–1311
- Redpath A T, Vickery B L and Wright D H 1976 A new technique for radiotherapy planning using quadratic programming *Phys. Med. Biol.* **21** 781–91
- Starkschall G 1984 A constrained least-squares optimization method for external beam radiation therapy treatment planning *Med. Phys.* **11** 659–65
- Sutlief S, Cho P and Phillips M 1998 Superposition kernels to compute dose from beam elements for inverse treatment planning *Med. Phys.* **25** A185
- van Santvoort J P C and Heijmen B J M 1996 Dynamic multileaf collimation without ‘tongue-and-groove’ underdosage effects *Phys. Med. Biol.* **41** 2091–105
- Xing L and Chen G T Y 1996 Iterative methods for inverse treatment planning *Phys. Med. Biol.* **41** 2107–23
- Webb S 1989 Optimization of conformal radiotherapy dose distributions by simulated annealing *Phys. Med. Biol.* **34** 1349–69